F2TNet: FMRI to T1w MRI Knowledge Transfer Network for Brain Multi-phenotype Prediction

Zhibin He[1], Wuyang Li[2], Yu Jiang[2], Zhihao Peng[2], Pengyu Wang[2], Xiang Li[4], Tianming Liu[3], Junwei Han[1], Tuo Zhang[1(✉)], Yixuan Yuan[2(✉)]

[1] School of Automation, Northwestern Polytechnical University, Xi'an, China
tuozhang@nwpu.edu.cn
[2] Department of Electronic Engineering, The Chinese University of Hong Kong, Hong Kong SAR, China
yxyuan@ee.cuhk.edu.hk
[3] Department of Computer Science, The University of Georgia, USA
[4] Massachusetts General Hospital and Harvard Medical School, USA

Abstract. Using brain imaging data to predict the non-neuroimaging phenotypes at the individual level is a fundamental goal of system neuroscience. Despite its significance, the *high acquisition cost* of functional Magnetic Resonance Imaging (fMRI) hampers its clinical translation in phenotype prediction, while the analysis based solely on cost-efficient T1-weighted (T1w) MRI yields *inferior performance* than fMRI. The reasons lie in that existing works ignore two significant challenges. 1) they neglect the knowledge transfer from fMRI to T1w MRI, failing to achieve effective prediction using cost-efficient T1w MRI. 2) They are limited to predicting a single phenotype and cannot capture the intrinsic dependence among various phenotypes, such as strength and endurance, preventing comprehensive and accurate clinical analysis. To tackle these issues, we propose an FMRI to T1w MRI knowledge transfer Network (F2TNet) to achieve *cost-efficient and effective* analysis on brain multi-phenotype, representing the first attempt in this field, which consists of a Phenotypes-guided Knowledge Transfer (PgKT) module and a modality-aware Multi-phenotype Prediction (MpP) module. Specifically, PgKT aligns brain nodes across modalities by solving a bipartite graph-matching problem, thereby achieving adaptive knowledge transfer from fMRI to T1w MRI through the guidance of multi-phenotype. Then, MpP enriches the phenotype codes with cross-modal complementary information and decomposes these codes to enable accurate multi-phenotype prediction. Experimental results demonstrate that the F2TNet significantly improves the prediction of brain multi-phenotype and outperforms state-of-the-art methods. The code is available at https://github.com/CUHK-AIM-Group/F2TNet.

Keywords: Brain phenotype prediction · Relationship between structure and function · Knowledge transfer.

Z. He—This work was done when Zhibin He was a visiting student at the Department of Electronic Engineering, The Chinese University of Hong Kong.

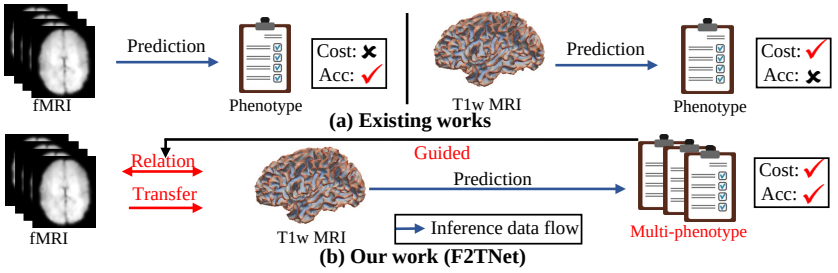

Fig. 1. (a) Prior works consistently rely on single modality data for predicting brain phenotype during inference. (b) The proposed F2TNet can achieve effective multi-phenotype prediction exclusively by utilizing cost-efficient T1w MRI during inference. For the specific multi-phenotype selection, please refer to the Preprocessing in Sec. 3.1.

1 Introduction

Using brain imaging data to predict non-neuroimaging phenotypes, such as fluid intelligence or clinical outcomes, is a fundamental goal of systems neuroscience [1,15]. Enhancing phenotype prediction not only augments our understanding of brain decoding but also establishes the foundation for disease diagnosis, precision medicine, and neuroscience research [2]. However, achieving precise phenotype prediction is challenging due to the complex relationships among brain structure, function, and phenotypes, as well as the individual-level variability [5,12,23,31].

Currently, existing works [3,6,7,23] have been proposed to address the mentioned challenge and can be divided into two categories according to the data modality used during inference. First, as shown in Fig. 1(a) left, numerous studies [3,6,7] focus on leveraging fMRI for phenotype prediction. They model brain regions as graph nodes, formulate graph edges with the correlations between brain regions' fMRI, and deploy graph convolutional networks for phenotype prediction. Despite achieving great successes, the high cost of fMRI data acquisition poses a significant barrier to its practical application in clinical settings [22]. Second, illustrated in Fig. 1(a) right, some effort [23] has been conducted to use cost-efficient T1w MRI for phenotype prediction. [23] extract brain surface information such as cortical thickness or curvature as brain region features and build regression models to predict phenotypes. Nevertheless, these results are inferior to fMRI-based data, primarily because the phenotype is relatively a more direct reflection of brain functions while the complex relationship between brain structure and function is not yet fully understood and mapped [4,10–12,28].

Despite some advancements, existing methods [3,6,7,23] fail to address both cost-efficient and effective simultaneously [14,19], due to two overlooked deficiencies. Firstly, they [3,6,7,23] neglect the knowledge transfer from fMRI to T1w MRI data, resulting in the inability to achieve effective prediction using cost-efficient T1w MRI data. Direct knowledge transfer between modalities may lead to suboptimal solutions due to the ambiguous relationship between brain structure and function [10–12,29]. Consequently, as illustrated in Fig. 1(b), our ob-

jective is to establish a good function-structure mapping for effective knowledge transfer from fMRI to T1w MRI data, enabling effective structure-to-phenotype prediction. Secondly, existing research [23] that solely utilizes T1w MRI for inference primarily concentrates on predicting a single phenotype, and cannot capture the intrinsic dependence among various phenotypes, such as strength and endurance, preventing comprehensive and accurate clinical analysis [29]. Therefore, as shown in Fig. 1(b), we aim to introduce a modality-aware multi-phenotype prediction, exploring the relationships between various phenotypes and imaging data, ensuring robust predictions for multi-phenotype.

To this end, we propose a novel FMRI to T1w MRI knowledge transfer Network (F2TNet) for cost-efficient and effective brain multi-phenotype prediction, which consists of a Phenotypes-guided Knowledge Transfer (PgKT) module, and a modality-aware Multi-phenotypes Prediction (MpP) module. Specifically, in the PgKT module, we align brain nodes across modalities by solving a bipartite graph-matching problem, thereby achieving adaptive knowledge transfer from fMRI to T1w MRI through the guidance of multi-phenotype. In the MpP module, we enrich the phenotype codes with cross-modal complementary information and decomposes these codes to enable accurate multi-phenotype prediction. Ultimately, during inference, we can achieve effective multi-phenotype prediction solely using T1w MRI. In summary, the main contributions are as follows: (1) We propose the F2TNet for cost-efficient and effective brain multi-phenotype prediction. To the best of our knowledge, this is the first attempt to achieve multi-phenotype prediction during inference using only T1w MRI. (2) We design a PgKT module to enable brain node alignment and knowledge transfer from fMRI to T1w MRI, and an MpP module to decompose modality-aware phenotype codes, achieving multi-phenotype prediction. (3) Experimental results demonstrate that the F2TNet significantly improves the prediction of multi-phenotype and outperforms state-of-the-art methods.

2 Method

The overview of our proposed network is shown in Fig. 2, which contains two parts. For a subject with N nodes of fMRI and T1w MRI data, and K phenotype labels denoted as $\mathbf{Y} \in \mathbb{R}^{1\times K}$, the fMRI and T1w MRI $\mathbf{P}_s, \mathbf{P}_t$ are independently input into the Vision Transformer (ViT) [19, 21] to obtain the respective features and phenotype codes. These are represented as $\mathbf{F}_s \in \mathbb{R}^{N\times d}, \mathbf{T}_s \in \mathbb{R}^{N\times d}$ for fMRI, and $\mathbf{F}_t \in \mathbb{R}^{N\times d}, \mathbf{T}_t \in \mathbb{R}^{K\times d}$ for T1w MRI. Subsequently, bipartite graph matching is employed for cross-modality node alignment, followed by modality knowledge transfer denoted as $\mathbf{F}_s^{'}, \mathbf{F}_t^{'}$, guided by phenotype codes in the PgKT module (Fig. 2(a), Sec. 2.1). Finally, the modality-aware phenotype codes $\mathbf{T}_s^{'}, \mathbf{T}_t^{'}$ are decomposed for multi-phenotype prediction, denoted as $\hat{\mathbf{Y}}$, in the MpP module (illustrated in Fig. 2(b), Sec. 2.2). The details will be introduced below.

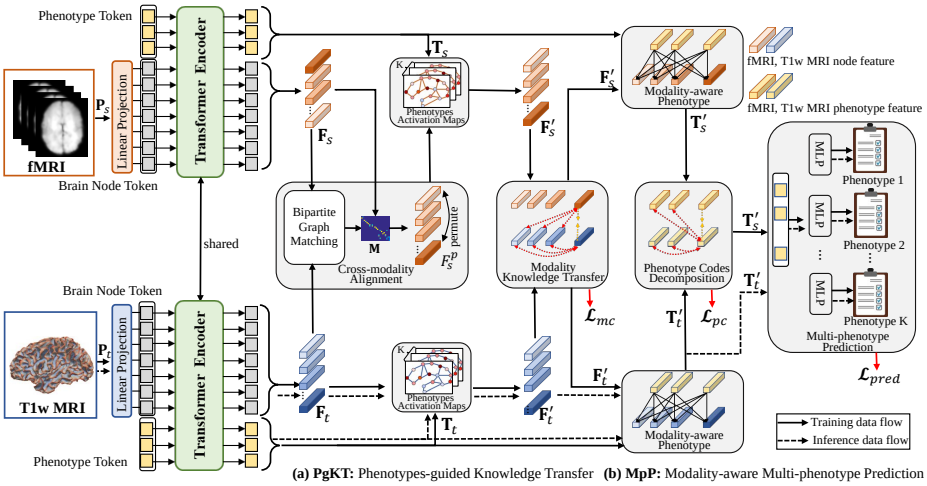

Fig. 2. Overview of the F2TNet. Notably, we solely utilize T1w MRI during inference.

2.1 Phenotypes-guided Knowledge Transfer (PgKT)

Cross-modality Alignment: As shown in Fig. 2(a), to augment cross-modality knowledge transfer, we propose bipartite graph matching to match nodes across modalities and permute fMRI nodes in a data-driven manner, thereby achieving modality alignment, instead of directly enforcing node alignment between modalities [25]. Firstly, we employ bipartite matching to ascertain a soft correspondence matrix between the two modalities, which is expressed as: $\mathbf{M} = \mathrm{Gbm}(\mathbf{F}_s, \mathbf{F}_t)$, where Gbm consists of an Affinity layer, an Instance normalization layer, a quadratic constrain (QC) layer, and a Sinkhorn layer. The affinity matrix is first computed as $\mathbf{A} = \mathbf{F}_s\mathbf{C}\mathbf{F}_t$, where $\mathbf{C} \in \mathbb{R}^{d\times d}$ is the learnable parameter matrix in the affinity layer. Subsequently, we apply instance normalization [11] to transform $\mathbf{A}$ into a matrix with positive elements within finite values. The QC is introduced to minimize the structural difference of matched node pairs [16,17,20], while the Sinkhorn layer [16] aids in calculating a double-stochastic affinity matrix through maximum iteration optimization, resulting in the soft assignment matrix $\mathbf{M}$. Secondly, we utilize the derived cross-modality brain node matching matrix $\mathbf{M}$ to permute the nodes of the fMRI $\mathbf{F}_s$, facilitating cross-modality alignment. This can be expressed as: $\mathbf{F}_s^p = \mathbf{F}_s\mathbf{M}$.

Modality Knowledge Transfer: Considering the diverse significance of different nodes in modality knowledge transfer, we incorporate the phenotype activation maps to discern the varying importance of nodes and enhance modality knowledge transfer in a data-driven manner. Specifically, we construct a phenotype activation maps, denoted as $\mathbf{H}_s, \mathbf{H}_t$, for data from the two modalities. The elements of this map indicate the importance of the n-th node within each modality for predicting the k-th phenotype. It can be expressed as follows: $\mathbf{H}_s = \mathbf{T}_s(\mathbf{F}_s^p)^T, \mathbf{H}_t = \mathbf{T}_t(\mathbf{F}_t)^T$, where $\mathbf{H}_s, \mathbf{H}_t \in \mathbb{R}^{K\times N}$. Guided by multi-

phenotype, we obtained the activated node features $\mathbf{F}_s^{'}, \mathbf{F}_t^{'}$, which is defined as:

$$\mathbf{F}_s^{'} = (\sum_{k=1}^{k=K} \mathbf{h}_{s,k}) @ \mathbf{F}_s^p, \mathbf{F}_t^{'} = (\sum_{k=1}^{k=K} \mathbf{h}_{t,k}) @ \mathbf{F}_t, \tag{1}$$

where $A@B$ represents the element-wise multiplication of A and B across each channel and $\mathbf{F}_s^{'}, \mathbf{F}_t^{'} \in \mathbb{R}^{N \times d}$. Subsequently, we conduct contrastive learning [30] across modalities of nodes to facilitate the transfer of knowledge. Our target is to guarantee that the corresponding nodes across different modalities exhibit similarity, while the non-corresponding nodes display distinct characteristics. Specifically, given an anchor fMRI node code $\boldsymbol{f}_{s,i}^{'}$, with i indicating the index of node, we regard codes $\boldsymbol{f}_{t,i}^{'}$ belonging to the matched node but different modalities as positive ones, and codes $\boldsymbol{f}_{t,j,j\neq i}^{'}$ belonging to other node as negative ones. To restrain the anchor codes and positive/negative codes via measuring their similarities, the modality knowledge transfer loss is formulated as follows:

$$\mathcal{L}_{\mathrm{mc}}^{i,j} = -\log \frac{h_\theta\left(\boldsymbol{f}_{s,i}^{'}, \boldsymbol{f}_{t,i}^{'}\right)}{h_\theta\left(\boldsymbol{f}_{s,i}^{'}, \boldsymbol{f}_{t,i}^{'}\right) + \sum_{j=1}^{N} 1_{[j\neq i]} h_\theta\left(\boldsymbol{f}_{s,i}^{'}, \boldsymbol{f}_{t,j}^{'}\right)}, \tag{2}$$

where $1_{[j\neq i]} \in 0, 1$ is an indicator function evaluating to 1 if $j \neq i$, and $h_\theta(.,.)$ denotes the affinity metric function and we adopt exponential cosine similarity $\mathcal{T}$ as: $h_\theta(\boldsymbol{p}, \boldsymbol{q}) = \exp\left(\frac{\boldsymbol{p}\cdot\boldsymbol{q}}{\|\boldsymbol{p}\|\cdot\|\boldsymbol{q}\|} \cdot \frac{1}{\mathcal{T}}\right)$, where $\mathcal{T}$ is the temperature factor facilitating the model to learn from hard negatives. Optimized by this contrastive loss, the model can directly transfer fMRI knowledge to T1w MRI data.

2.2 Modality-aware Multi-phenotype Prediction (MpP)

Modality-aware Phenotype Codes Decomposition: As shown in Fig. 2(b), we employ cross-attention [27] to enrich the phenotype codes with cross-modality complementary information, thereby obtaining modality-aware phenotype codes. The attention layer selects the information between phenotype codes by measuring the similarity between the query $\mathbf{Q}$ and the key $\mathbf{K}$. The output vector is the sum of the value $\mathbf{V}$ weighted by the similarity scores. The multi-head attention layer is defined as $\mathrm{MHAttn}(\mathbf{Q}, \mathbf{K}, \mathbf{V})$, $\mathbf{Q}$ comes from the phenotype codes, $\mathbf{K}$ and $\mathbf{V}$ come from the brain node codes. The outputs of Cross-attention are: $\mathbf{T}_s^{'} = \mathrm{MHAttn}(\mathbf{T}_s, \mathbf{F}_s^{'}, \mathbf{F}_s^{'}), \mathbf{T}_t^{'} = \mathrm{MHAttn}(\mathbf{T}_t, \mathbf{F}_t^{'}, \mathbf{F}_t^{'})$. Subsequently, we implement contrastive learning on modality-aware phenotype codes to accomplish inter-phenotype decomposition. Given a modality phenotype code $\boldsymbol{t}_{s,i}^{'}$, as the anchor, phenotype code belonging to the same phenotype but different modality are regarded as positive ones $\boldsymbol{t}_{t,i}^{'}$, and phenotype code belonging to other modality and other phenotype are regarded as negative ones $\boldsymbol{t}_{t,j,j\neq i}^{'}$, the formulation of the phenotype contrastive loss is as follows:

$$\mathcal{L}_{\mathrm{pc}}^{i,j} = -\log \frac{h_\theta\left(\boldsymbol{t}_{s,i}^{'}, \boldsymbol{t}_{t,i}^{'}\right)}{h_\theta\left(\boldsymbol{t}_{s,i}^{'}, \boldsymbol{t}_{t,i}^{'}\right) + \sum_{j=1}^{N} 1_{[j\neq i]} h_\theta\left(\boldsymbol{t}_{s,i}^{'}, \boldsymbol{t}_{t,j}^{'}\right)}, \tag{3}$$

where $\boldsymbol{t}^{'}_{s,i}$, $\boldsymbol{t}^{'}_{t,i}$, and $\boldsymbol{t}^{'}_{t,j,j\neq i}$ are anchor, positive and negative phenotype code.
Multi-phenotype Prediction: To predict multi-phenotype, we employ multi multi-layer perceptron (MLP) to build predictor for each phenotype. This can be expressed as: $\hat{\mathbf{Y}} = \sigma(\mathbf{T}^{'}_{s}\boldsymbol{\Theta})$, where $\boldsymbol{\Theta}$ denotes the learnable parameters of predictor, $\sigma(\cdot)$ is the nonlinear activation function. Ultimately, we employ mean squared error (MSE) loss function to calculate the cost between the ground truth and the predicted multi-phenotype. The prediction loss is defined as follows:

$$\mathcal{L}_{\text{pred}} = MSE(\hat{\mathbf{Y}}, \mathbf{Y}) \tag{4}$$

2.3 Model Optimization:

In the training of this work, we introduce hyperparameters α and β to add up $\mathcal{L}_{\text{pred}}$, $\mathcal{L}_{\text{mc}}$, and $\mathcal{L}_{\text{pc}}$. Then, the overall train loss is denoted as follows:

$$\mathcal{L} = \mathcal{L}_{\text{pred}} + \alpha\mathcal{L}_{\text{mc}} + \beta\mathcal{L}_{\text{pc}}, \tag{5}$$

where α and β are hyperparameters to control the intensity. During inference, precise multi-phenotype prediction is achievable solely using T1w MRI data.

3 Experiments and Results

3.1 Experimental setup

Dataset: We evaluate our network effectiveness by conducting experiments on the WU-Minn Human Connectome Project (HCP) consortium [26]. HCP participants gave written informed consent, and the relevant institutional review boards approved the study. For detailed imaging data parameter, please see [26].
Preprocessing: T1w MRI and resting state fMRI have been preprocessed by the HCP minimal preprocessing pipeline [8]. Utilizing the Gordon atlas [9], 333 cortical regions are derived for each subject. For the fMRI, we compute the average signals of vertices within cortical regions, constructing a 333×333 functional connectivity matrix $\mathbf{P}_s$ based on Pearson correlations. Negative correlations are eliminated, along with 90% of the weakest positive correlations. The row vectors of $\mathbf{P}_s$ represent features of each node [7]. For the T1 MRI, we calculate the mean curvature, convexity, cortical thickness, correlation thickness, edge distortion, area distortion, sphere distortion, bias field, smooth myelin map within each region based on the surface and construct a 333×9 structural feature matrix $\mathbf{P}_t$. The row vectors of this matrix $\mathbf{P}_t$ are treated as the features of each node. Given that the phenotype spans multiple domains, we selected a total of twelve phenotypes (#1: VSPLOT_TC, #2: ReadEng_Unadj, #3: PercStress_Unadj, #4: AngAggr_Unadj, #5: Strength_Unadj, #6: Endurance_Unadj, #7: PicVocab_Unadj, #8: ListSort_Unadj, #9: AngHostil_Unadj, #10: Loneliness_Unadj, #11: MeanPurp_Unadj, #12: Dexterity_Unadj) across the three domains of cognition, emotion, and motor. The phenotypes are individually normalized to the range [0, 1] using the minimum and maximum values [6].

Table 1. Comparison with state-of-the-art methods (based on PCC and RMSE). Infer. denotes the data needed for inference, S/M indicates whether it predicts a **S**ingle- or **M**ulti-phenotype, and #1-#6 represent different phenotypes. Light blue shading indicates the use of only T1w MRI during inference, and the best results are **highlighted**.

Method	Row	Train	Infer.	S / M	Phenotypes											
					Metric: PCC (10^{-1}) ↑						Metric: RMSE (10^{-1}) ↓					
					#1	#2	#3	#4	#5	#6	#1	#2	#3	#4	#5	#6
Brain GNN [18]	1	fMRI	fMRI	S	2.23	2.19	1.18	2.63	2.75	2.07	2.45	2.78	2.63	3.84	3.30	3.60
	2	T1w	T1w	S	1.02	0.43	0.16	0.21	1.13	1.07	3.42	3.74	2.95	5.35	3.20	4.36
SaU-B Net [3]	3	fMRI	fMRI	S	2.31	2.57	1.53	2.52	2.74	2.53	2.41	2.33	2.44	3.91	3.34	3.01
	4	T1w	T1w	S	0.98	0.45	0.22	0.28	1.31	1.01	3.44	3.78	2.91	5.27	3.21	4.34
KRR [23]	5	fMRI	fMRI	S	2.37	2.28	1.07	2.61	2.81	2.31	2.37	2.63	2.66	3.84	3.27	2.88
	6	T1w	T1w	S	1.11	0.77	0.19	0.27	1.22	1.13	3.29	3.21	3.07	5.31	3.19	4.07
At-Cen Net [7]	7	fMRI	fMRI	S	2.27	2.34	1.37	2.66	2.69	2.40	2.44	2.42	2.57	3.84	3.41	2.73
	8	T1w	T1w	S	0.96	0.54	0.22	0.31	1.09	1.15	3.51	3.53	2.93	5.20	3.35	4.01
Our	9	fMRI	fMRI	S	2.57	3.16	1.89	3.12	2.98	3.07	2.27	2.14	2.48	3.21	2.93	2.27
	10	T1w	T1w	S	1.22	0.54	0.25	0.65	1.33	1.16	3.23	3.49	2.89	4.08	3.13	4.03
	11	fMRI	fMRI	M	2.47	3.11	1.91	2.97	2.73	2.96	2.28	2.21	2.54	3.19	3.01	2.33
	12	T1w	T1w	M	1.18	0.47	0.33	0.39	1.29	1.04	3.34	3.71	2.93	4.07	3.20	4.11
	13	fMRI, T1w	T1w	M	**2.27**	**2.77**	**1.50**	**1.56**	**3.54**	**2.97**	**2.30**	**2.20**	**2.42**	**3.92**	**2.01**	**2.38**

Evaluation: We adopt the Pearson's correlation coefficient (PCC) and root mean square error (RMSE) between the ground truth and predicted values as evaluation metrics for our proposed model [6]. To evaluate the performance of our model, we compare it against several state-of-the-art phenotype prediction methods, including BrainGNN [18], SaU-BNet [3], KRR [23], and At-CenNet [7]. Notably, we exclude comparisons with non-open-source methods such as [6].
Implementation Details: We utilize the Adam optimizer [13] with 3×10^{-5} learning rate, $5{\times}10^{-4}$ weight decay, 10 batch size, and 100 epochs. Our model utilizes a ViT architecture with 3 depths, 333 node tokens, and 6 phenotype tokens. We set the hyperparameters α=0.8, and β=1, the feature channel d=2048. We implement our network using the PyTorch library [24]. Among the 870 subjects, 5 subjects are excluded due to missing phenotype measures. From the remaining subjects, we randomly select 525/170/170 for training/validation/testing.

3.2 Experimental Results

Comparison with State-of-the-arts: The comparative results of phenotypes #1-#6 are presented in Table 1. When predicting solely with T1w MRI (indicated by light blue shading) during inference, our approach demonstrates superior performance across both PCC and RMSE (13^{th} row). Simultaneous prediction of six phenotypes yields an average PCC=0.24 ± 0.081 and RMSE=0.25 ± 0.069, surpassing existing methods [3, 18, 23]. These results demonstrate that our method successfully transfers knowledge from fMRI to T1w MRI and decomposes phenotype codes. F2TNet outperforms even when only fMRI is utilized (9^{th} row). This not only substantiates that fMRI indeed encapsulates

Table 2. The impact of each component of our proposed F2TNet on the prediction performance (based on PCC and RMSE). The best results are **highlighted**.

Components	Phenotypes											
	Metric: PCC (10^{-1}) ↑						Metric: RMSE (10^{-1})) ↓					
	#1	#2	#3	#4	#5	#6	#1	#2	#3	#4	#5	#6
w/o Node Alignment	1.99	2.49	1.31	1.35	3.11	2.68	2.41	2.33	2.49	4.21	2.19	2.41
w/o Modality-aware Phenotype	2.11	2.63	1.49	1.47	3.02	2.68	2.33	2.29	2.53	3.97	2.05	2.47
w/o $\mathcal{L}_{pc}$	0.97	0.54	0.82	1.01	2.11	0.99	3.41	3.68	3.41	2.97	3.21	4.08
Our	**2.27**	**2.77**	**1.50**	**1.56**	**3.54**	**2.97**	**2.30**	**2.20**	**2.42**	**3.92**	**2.01**	**2.38**

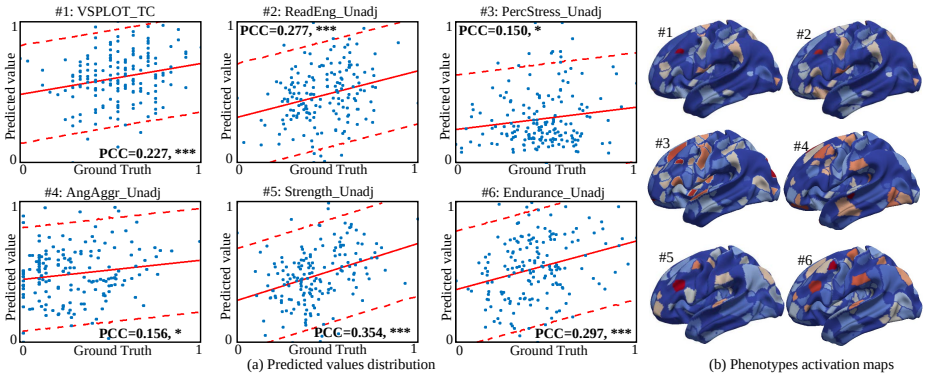

Fig. 3. (a) The distribution of predicted values for the six phenotypes. * denote the P-value<0.05, and *** denote the P-value<0.0005. The red line represents a linearly fitted trend line. The red dashed lines contain the 90% prediction interval. (b) The visualization results of phenotype active maps based on Gordon atlas.

more information but also verifies that our approach can yield more precise predictions. In addition, we sequentially exclude two phenotypes for predicting four phenotypes simultaneously in 15 experiments, resulting in an average PCC=0.25 ± 0.075 and RMSE=0.24 ± 0.064. Subsequently, using phenotypes #7-#12 for predicting all six phenotypes simultaneously, the average PCC=0.22 ± 0.084, the RMSE=0.26 ± 0.074, and it outperforms state-of-the-art methods, demonstrating the effectiveness and robustness of our method.

Ablation Studies: Table 2 displays ablation studies that verify the efficacy of each component of the proposed F2TNet. Taking Phenotype #1 as an example, our findings underscore the importance of aligning cross-modality brain nodes in a data-driven manner, evident from the impact on PCC when node alignment is omitted (PCC=0.20). Introducing the modality-aware phenotype enhances the PCC, with modality-aware phenotype removal leading to PCC=0.21. Removing the phenotype codes decomposition loss resulted in PCC=0.097, suggesting that the decomposition of phenotype codes significantly enhances prediction accuracy. Hence, each component is necessary for the F2TNet to achieve precise results.

Qualitative Analysis: Fig. 3(a) shows the distribution of predicted values and true values for 6 phenotypes, showcasing high correlations and successful multi-phenotype prediction using cost-efficient T1w MRI. In Fig. 3(b), the pheno-

type activation maps for #1-#6 reveal similar activation regions for phenotypes within the same domain (#1/#2, #3/#4, #5/#6), indicating our method's ability to capture inherent dependencies among phenotypes in the same domain.

4 Conclusion

In this paper, we propose a novel network F2TNet for cost-efficient and effective brain multi-phenotype prediction. F2TNet consists of a PgKT module to enable brain node alignment and knowledge transfer from fMRI to T1w MRI through the guidance of multi-phenotype, and an MpP module to decompose modality-aware phenotype codes, achieving multi-phenotype prediction. Experimental results demonstrate that F2TNet outperforms existing approaches significantly.

Acknowledgment. This work was supported in part by Hong Kong Research Grants Council (RGC) General Research Fund 14204321, and in part by the National Natural Science Foundation of China 62131009.

Disclosure of Interests. The authors have no competing interests to declare that are relevant to the content of this article.

References

1. Biswal, B., Zerrin Yetkin, F., Haughton, V.M., Hyde, J.S.: Functional connectivity in the motor cortex of resting human brain using echo-planar mri. Magnetic resonance in medicine **34**(4), 537–541 (1995)
2. Buckner, R.L., Krienen, F.M., Yeo, B.T.: Opportunities and limitations of intrinsic functional connectivity mri. Nature neuroscience **16**(7), 832–837 (2013)
3. Chen, J., Tam, A., Kebets, V., Orban, C., Ooi, L.Q.R., Asplund, C.L., Marek, S., Dosenbach, N.U., Eickhoff, S.B., Bzdok, D., et al.: Shared and unique brain network features predict cognitive, personality, and mental health scores in the abcd study. Nature communications **13**(1), 1–17 (2022)
4. Chen, W., Liu, Y., Hu, J., Yuan, Y.: Dynamic depth-aware network for endoscopy super-resolution. IEEE Journal of Biomedical and Health Informatics **26**(10), 5189–5200 (2022)
5. Chen, Z., Li, W., Xing, X., Yuan, Y.: Medical federated learning with joint graph purification for noisy label learning. Medical Image Analysis **90**, 102976 (2023)
6. Cheng, J., Zhang, X., Zhao, F., Wu, Z., Yuan, X., Wang, L., Lin, W., Li, G.: Prediction of infant cognitive development with cortical surface-based multimodal learning. In: International Conference on Medical Image Computing and Computer-Assisted Intervention. pp. 618–627. Springer (2023)
7. Gao, J., Zhao, L., Zhong, T., Li, C., He, Z., Wei, Y., Zhang, S., Guo, L., Liu, T., Han, J., et al.: Prediction of cognitive scores by joint use of movie-watching fmri connectivity and eye tracking via attention-censnet. Psychoradiology **3** (2023)
8. Glasser, M.F., Sotiropoulos, S.N., Wilson, J.A., Coalson, T.S., Fischl, B., Andersson, J.L., Xu, J., Jbabdi, S., Webster, M., Polimeni, J.R., et al.: The minimal preprocessing pipelines for the human connectome project. Neuroimage **80**, 105–124 (2013)

9. Gordon, E.M., Laumann, T.O., Adeyemo, B., Huckins, J.F., Kelley, W.M., Petersen, S.E.: Generation and evaluation of a cortical area parcellation from resting-state correlations. Cerebral cortex **26**(1), 288–303 (2016)
10. He, Z., Du, L., Huang, Y., Jiang, X., Lv, J., Guo, L., Zhang, S., Zhang, T.: Gyral hinges account for the highest cost and the highest communication capacity in a corticocortical network. Cerebral Cortex **32**(16), 3359–3376 (2022)
11. He, Z., Li, W., Zhang, T., Yuan, Y.: H 2 gm: A hierarchical hypergraph matching framework for brain landmark alignment. In: International Conference on Medical Image Computing and Computer-Assisted Intervention. pp. 548–558. Springer (2023)
12. Jiang, X., Zhang, T., Zhang, S., Kendrick, K.M., Liu, T.: Fundamental functional differences between gyri and sulci: implications for brain function, cognition, and behavior. Psychoradiology **1**(1), 23–41 (2021)
13. Kingma, D.P., Ba, J.: Adam: A method for stochastic optimization. arXiv preprint arXiv:1412.6980 (2014)
14. Li, C., Lin, M., Ding, Z., Lin, N., Zhuang, Y., Huang, Y., Ding, X., Cao, L.: Knowledge condensation distillation. In: European Conference on Computer Vision. pp. 19–35. Springer Nature Switzerland Cham (2022)
15. Li, J., Kong, R., Liégeois, R., Orban, C., Tan, Y., Sun, N., Holmes, A.J., Sabuncu, M.R., Ge, T., Yeo, B.T.: Global signal regression strengthens association between resting-state functional connectivity and behavior. NeuroImage **196**, 126–141 (2019)
16. Li, W., Liu, X., Yuan, Y.: Sigma: Semantic-complete graph matching for domain adaptive object detection. In: Proceedings of the IEEE/CVF Conference on Computer Vision and Pattern Recognition. pp. 5291–5300 (2022)
17. Li, W., Liu, X., Yuan, Y.: Sigma++: Improved semantic-complete graph matching for domain adaptive object detection. IEEE Transactions on Pattern Analysis and Machine Intelligence (2023)
18. Li, X., Zhou, Y., Dvornek, N., Zhang, M., Gao, S., Zhuang, J., Scheinost, D., Staib, L.H., Ventola, P., Duncan, J.S.: Braingnn: Interpretable brain graph neural network for fmri analysis. Medical Image Analysis **74**, 102233 (2021)
19. Liu, X., Peng, H., Zheng, N., Yang, Y., Hu, H., Yuan, Y.: Efficientvit: Memory efficient vision transformer with cascaded group attention. In: Proceedings of the IEEE/CVF Conference on Computer Vision and Pattern Recognition. pp. 14420–14430 (2023)
20. Liu, Y., Li, W., Liu, J., Chen, H., Yuan, Y.: Grab-net: Graph-based boundary-aware network for medical point cloud segmentation. IEEE Transactions on Medical Imaging (2023)
21. Liu, Y., Liu, J., Yuan, Y.: Edge-oriented point-cloud transformer for 3d intracranial aneurysm segmentation. In: International Conference on Medical Image Computing and Computer-Assisted Intervention. pp. 97–106. Springer (2022)
22. Nickerson, L.D.: Replication of resting state-task network correspondence and novel findings on brain network activation during task fmri in the human connectome project study. Scientific reports **8**(1), 17543 (2018)
23. Ooi, L.Q.R., Chen, J., Zhang, S., Kong, R., Tam, A., Li, J., Dhamala, E., Zhou, J.H., Holmes, A.J., Yeo, B.T.: Comparison of individualized behavioral predictions across anatomical, diffusion and functional connectivity mri. NeuroImage **263**, 119636 (2022)
24. Paszke, A., Gross, S., Massa, F., Lerer, A., Bradbury, J., Chanan, G., Killeen, T., Lin, Z., Gimelshein, N., Antiga, L., et al.: Pytorch: An imperative style, high-

performance deep learning library. Advances in neural information processing systems **32** (2019)
25. Sebenius, I., Campbell, A., Morgan, S.E., Bullmore, E.T., Liò, P.: Multimodal graph coarsening for interpretable, mri-based brain graph neural network. In: 2021 IEEE 31st International Workshop on Machine Learning for Signal Processing (MLSP). pp. 1–6. IEEE (2021)
26. Van Essen, D.C., Smith, S.M., Barch, D.M., Behrens, T.E., Yacoub, E., Ugurbil, K., Consortium, W.M.H., et al.: The wu-minn human connectome project: an overview. Neuroimage **80**, 62–79 (2013)
27. Vaswani, A., Shazeer, N., Parmar, N., Uszkoreit, J., Jones, L., Gomez, A.N., Kaiser, Ł., Polosukhin, I.: Attention is all you need. Advances in neural information processing systems **30** (2017)
28. Wang, Q., Zhao, S., He, Z., Zhang, S., Jiang, X., Zhang, T., Liu, T., Liu, C., Han, J.: Modeling functional difference between gyri and sulci within intrinsic connectivity networks. Cerebral Cortex **33**(4), 933–947 (2023)
29. Wang, Q., Zhao, S., Liu, T., Han, J., Liu, C.: Temporal fingerprints of cortical gyrification in marmosets and humans. Cerebral Cortex **33**(17), 9802–9814 (2023)
30. Yang, Q., Guo, X., Chen, Z., Woo, P.Y., Yuan, Y.: D 2-net: Dual disentanglement network for brain tumor segmentation with missing modalities. IEEE Transactions on Medical Imaging **41**(10), 2953–2964 (2022)
31. Zhang, S., Zhang, T., Cao, G., Zhou, J., He, Z., Li, X., Ren, Y., Liu, T., Jiang, X., Guo, L., et al.: Species-shared and-unique gyral peaks on human and macaque brains. Elife **12**, RP90182 (2024)